ECS Journal of Solid State
Science and Technology

Thermal Stability of Transparent ITO/n-Ga_2O_3/n+-Ga_2O_3/ITO Rectifiers

ECS Journal of Solid State Science and Technology, 2021 **10** 115005
2162-8777/2021/10(11)/115005/8/$40.00 © 2021 The Electrochemical Society ("ECS"). Published on behalf of ECS by IOP Publishing Limited

Thermal Stability of Transparent ITO/n-Ga_2O_3/n+-Ga_2O_3/ITO Rectifiers

Xinyi Xia,[1,*] Minghan Xian,[1,*] Fan Ren,[1,] Md Abu Jafar Rasel,[2] Aman Haque,[2] and S. J. Pearton[3,**,z]**

[1]*Department of Chemical Engineering, University of Florida, Gainesville, Florida 32611, United States of America*
[2]*Department of Mechanical Engineering, The Pennsylvania State University, University Park, Pennsylvania 16802, United States of America*
[3]*Department of Materials Science and Engineering, University of Florida, Gainesville, Florida 32611 United States of America*

The thermal stability of n/n$^+$ β-Ga_2O_3 epitaxial layer/substrate structures with sputtered ITO on both sides to act as rectifying contacts on the lightly doped layer and Ohmic on the heavily doped substrate is reported. The resistivity of the ITO deposited separately on Si decreased from 1.83×10^{-3} Ω.cm as-deposited to 3.6×10^{-4} Ω.cm after 300 °C anneal, with only minor reductions at higher temperatures (2.8×10^{-4} Ω.cm after 600 °C anneals). The Schottky barrier height also decreased with annealing, from 0.98 eV in the as-deposited samples to 0.85 eV after 500 °C annealing. The reverse breakdown voltage exhibited a negative temperature coefficient of -0.46 V.C^{-1} up to an annealing temperature of 400 °C and degraded faster at higher temperatures. Transmission Electron Microscopy showed significant reaction at the ITO and Ga_2O_3 interface above 300 °C, with a very degraded contact stack after annealing at 500 °C.
 [DOI: 10.1149/2162-8777/ac3ace]

Manuscript submitted September 14, 2021; revised manuscript received October 28, 2021. Published November 26, 2021.

Ga_2O_3 is attracting interest for high power rectifiers in inverter systems for renewable energy sources and rapid chargers for electric vehicles.[1–13] There are also applications where transparent contacts on Ga_2O_3 electronic devices would be advantageous, including optical triggering of power switches and having the ability to probe single event radiation upsets using laser pulses to simulate heavy ion single events effects (SEE).[4–21] Ga_2O_3 based devices have the potential to achieve better efficiencies than SiC or GaN devices due to the higher breakdown field.[1–5,8–10] However, while Ga_2O_3 can operate to at least 350 °C,[9,11] many of the gate dielectrics employed react at ~200 °C,[10] and packaging has also yet to match the high operating temperatures achieved in the more mature wide bandgap semiconductors.[10] The integrated gate in common thyristor designs creates a channel for power loss directly into the control electronics. An optically-controlled gate would add flexibility to these devices allowing them to be used to their full potential.[14] A key component of high efficiency power devices could be realized by the integration of SiC base structures with epitaxially grown Ga_2O_3 gates for high power optically controlled devices.

Similarly, it is typical in SEE testing to irradiate the device under test with different ions (e.g., H, C through Ni) to produce different linear energy transfer (LET) heavy ions at energies up to 25 MeV (LET ~ 30 MeV/(mg cm^{-2}) to simulate the response to cosmic/solar radiation.[14–21] Since this is expensive and time-consuming, pulsed X-ray or laser approaches have been developed to separate the combined effects of ionization and displacement damage processes.[14–21] Both single-photon absorption (SPA) and two-photon absorption (TPA) pulsed-laser systems allow for rapid-feedback of radiation studies at lower costs than conventional heavy-ion broad beam testing. These alternative SEE testing methods show promise for basic research and would benefit from simple transparent Schottky contacts to allow for the injection of charge from laser pulses into the Ga_2O_3.

ITO is a promising transparent contact for Ga_2O_3,[22–29] especially since it behaves as a rectifying contact on lightly n-type material and as an Ohmic contact on heavily n$^+$ Ga_2O_3.[30,31] Even though the bandgap (~4 eV) is lower than that of Ga_2O_3 there are generally enough below gap states to allow changes in conductivity through excitation of these gap states and a thin ITO Schottky contact would still be much more transparent than a conventional metal contact. We have previously found that sputtered ITO Schottky contacts are thermally stable up to 500 K and suffer irreversible thermal damage at 600 K.[30] The effect of temperature on conventional Ti/Au Ohmic contacts has been reported, showing they are unstable at 350 °C.[32–34] Other reports have shown that part of this degradation is due to migration and oxidation of Ti at the top surface of the Au contact pads.[35–50] However, there is little known about the stability of ITO contacts on Ga_2O_3. In this paper we describe the stability of transparent ITO/n-Ga_2O_3/n$^+$-Ga_2O_3/ ITO rectifiers to annealing up to 500 °C.

Experimental

The drift region of the structure consisted of a 10 μm thick, lightly Si doped epitaxial layer grown by halide vapor phase epitaxy (HVPE) with carrier concentration of 3×10^{16} cm^{-3}, and this epitaxial layer was grown on a (001) orientation, 2-inch diameter Sn-doped ($n = 10^{19}$ cm^{-3}) β-Ga_2O_3 single crystal (Novel Crystal Technology, Japan). The wafer surfaces were ultrasonically cleaned in acetone, methanol, and isopropyl alcohol.

A full area, 75 nm thick ITO backside Ohmic contact was formed by dc sputtering at room temperature using a 3-in. target of ITO. The dc power was 125 W and the process pressure was 5 mTorr in pure Argon ambient. We also deposited 200 nm ITO under the same conditions on sentinel Si wafers to allow us to measure the resistivity as a function of anneal temperature up to 600 °C under either O_2 or N_2 ambients. After backside Ohmic formation, the front of the sample was cleaned using HCl and then treated with ozone for 20 minutes to remove residual hydrocarbons. Next, the sample was patterned for Schottky contact formation. A 75 nm ITO layer was similarly deposited by dc sputtering. Edge termination was not used, in order to focus on the ITO contact characteristics free of edge effects. Figure 1a shows a plan view optical microscope image schematic of the competed devices, with circular contact diameters of 50–200 μm and square contacts of length 400 μm. We included different contact sizes and shapes so we could examine the effect of current density and geometry on the breakdown characteristics of the ITO contacts, since this has been an issue with conventional contacts.[51] There was no clear dependence of forward and reverse current densities over the range of contact sizes investigated and nor was there a difference between circular and square geometries. Figure 1c shows an optical microscope image of the fabricated diodes with ITO on both sides to provide contacts to the

*Electrochemical Society Student Member.
**Electrochemical Society Fellow.
zE-mail: spear@mse.ufl.edu

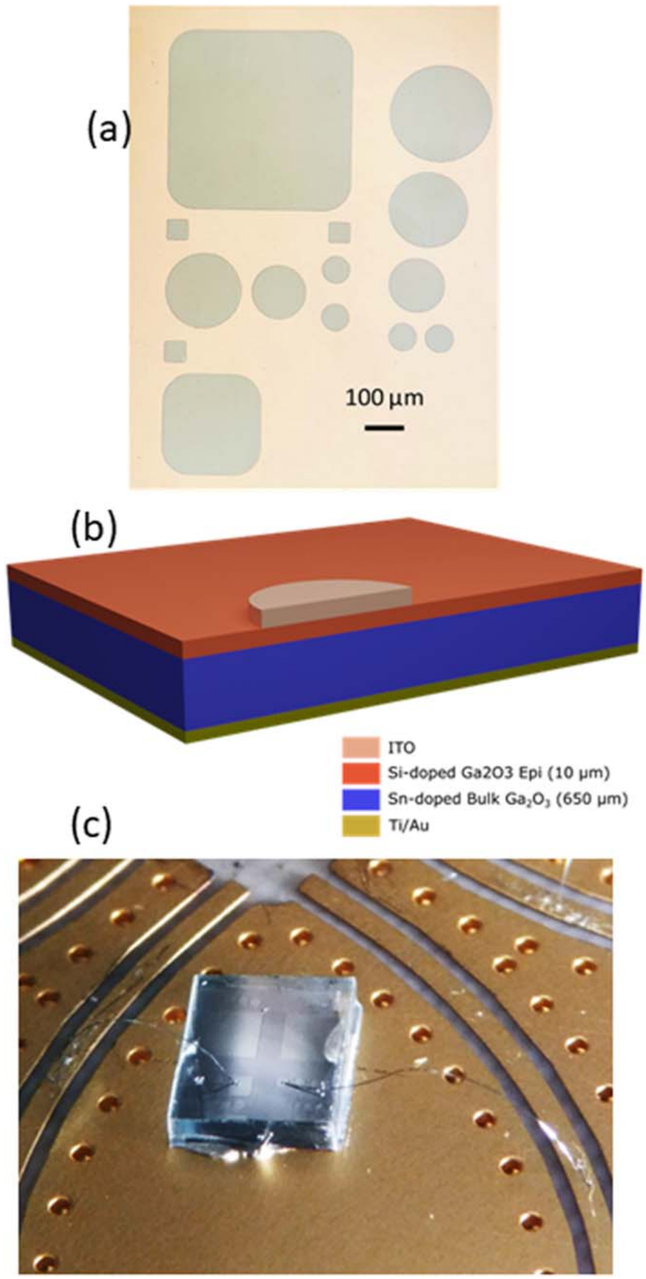

Figure 1. (a) Plan view optical image of front-side ITO Schottky contacts (b) schematic of entire structure and (c) photograph of transparent ITO/n-Ga_2O_3/n$^+$-Ga_2O_3/ ITO rectifier.

Table I. Four-point measurement data, 200 nm ITO on silicon wafer.

	Spot 1	Spot 2	Spot 3	Average Ω/□	Resistivity Ω.cm
Reference	93.7	90	90.2	91.3	1.83×10^{-3}
300 °C, N_2	18.01	17.85	18.3	18.1	3.6×10^{-4}
400 °C, N_2	16.7	17.5	17.5	17.2	3.4×10^{-4}
500 °C, N_2	14	13.5	13.5	13.7	2.7×10^{-4}
600 °C, N_2	14.78	13.9	13.5	14.0	2.8×10^{-4}
600 °C, O_2	424.8	423.2	424.0	424.0	8.5×10^{-3}

n-Ga_2O_3/n$^+$-Ga_2O_3 rectifier structure. These were annealed under N_2 at temperatures up to 500 °C.

The current-voltage (I-V) characteristics were recorded were recorded with a HP 4156 parameter analyzer for forward bias and with a Tektronix 370-A curve tracer for reverse bias. We measured 4–5 different diodes for each condition, with the results being within 5% within this distribution. The forward current characteristic was used to extract the zero-bias equivalent barrier height (Φ_b) and ideality factor (n) from the relationship for current density in TE theory, given by[32,42,45]

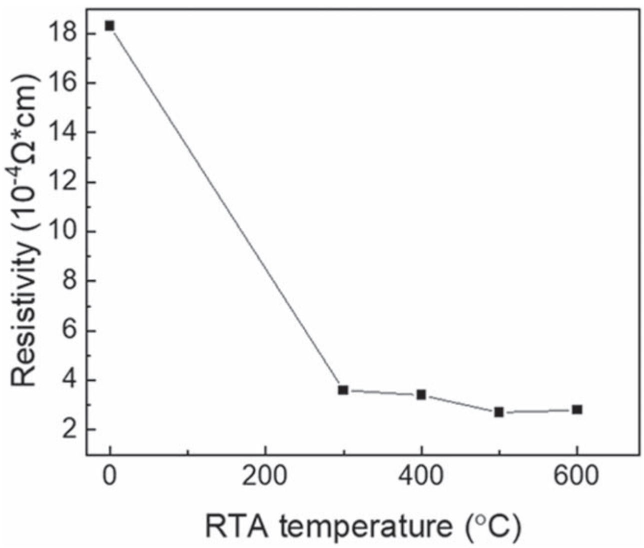

Figure 2. Resistivity of 200 nm thick ITO deposited on Si, as a function of subsequent annealing temperature in N_2 ambient.

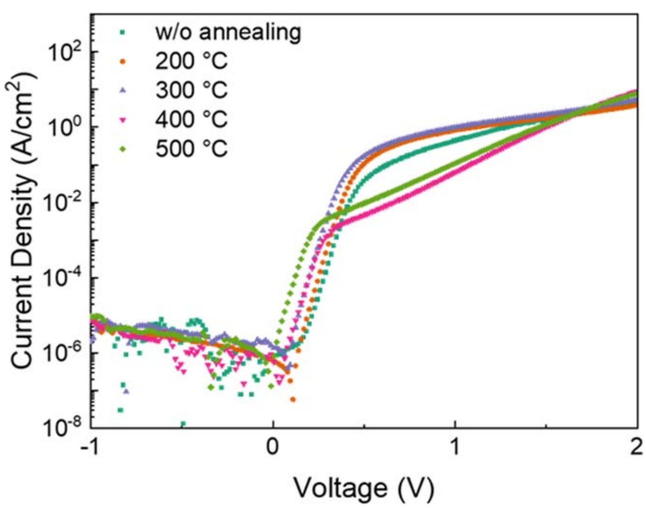

Figure 3. Forward I-V characteristics of ITO/n-Ga_2O_3/n$^+$-Ga_2O_3/ ITO rectifier as a function of annealing temperature in N_2 ambient.

$$J = J_0 \exp(eV_A/nkT)\,[1 - \exp(-eV_A/kT)$$

where $J_0 = A^* m_{eff}/m_0 T^2 \exp(\Phi_B/kT)$, e is electronic charge and A^* is the Richardson constant (33.7 $A.cm^{-2}K^{-2}$) and V_A is the bias voltage applied. The values of barrier height were corrected for the image force (IF) lowering, as described elsewhere and also represent the average of 4–5 different diodes at each condition.[32] The ideality factors, n, of the diodes were extracted from the slope of the linear part of the subthreshold region for each temperature assuming thermionic emission dominates, i.e. $n = (e/kT)\,(dV_D/d\ln(J_D/J_0))$.

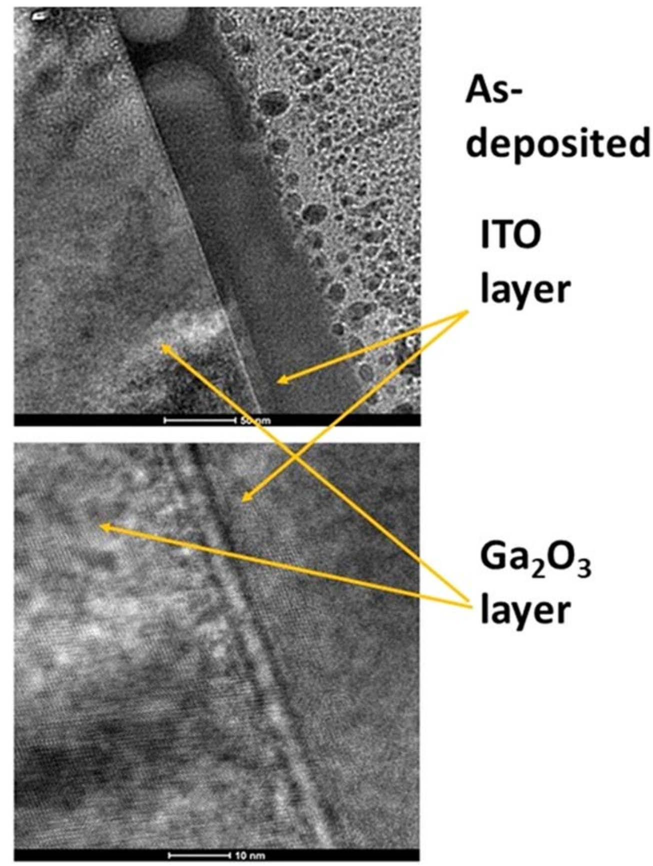

Figure 4. TEM cross-sectional images of the ITO/Ga_2O_3 interfaces after annealing at different temperatures.

The diode on/off ratio was measured when switching from 3 V forward to reverse biases up to 100 V. The reverse breakdown voltage was defined as the bias for a reverse current reached before 3 mA.

The structural stability of the ITO/Ga_2O_3 structures was examined by cross-sectional Transmission Electron Microscopy (TEM) and Energy Dispersive X-ray Spectroscopy (EDS) to measure interfacial stability and map the elemental composition near the interface.

Results and Discussion

Figure 2 and Table I show the evolution of ITO resistivity with annealing temperature. The trends are typical of what has been reported previously by a number of groups,[23–29] with a sharp decrease up to 300 °C and a saturation at higher temperatures. For annealing in O_2, the reaction will decrease the oxygen vacancies and the carrier concentration, which results in the increase of the resistivity of the films relative to annealing in N_2 ambients.[23–29]

Figure 3 shows the forward I-V characteristics before and after annealing. The shape of the curves and magnitude of the forward current is degraded after annealing above 300 °C, suggesting the

Table II. Barrier height, ideality factor, reverse breakdown voltage and currents at breakdown, as a function of annealing temperature.

	Schottky barrier height	Ideality factor	Breakdown voltage (V)	Current (A)	Current density (A cm^{-2})
w/o annealing	0.98	1.06	416	1.52×10^{-7}	1.94×10^{-3}
200 °C	0.99	1.03	320	6.26×10^{-7}	7.97×10^{-3}
300 °C	0.93	1.04	282	8.48×10^{-7}	1.08×10^{-2}
400 °C	0.93	1.07	244	7.67×10^{-7}	9.77×10^{-3}
500 °C	0.85	1.12	122	7.95×10^{-7}	1.01×10^{-2}

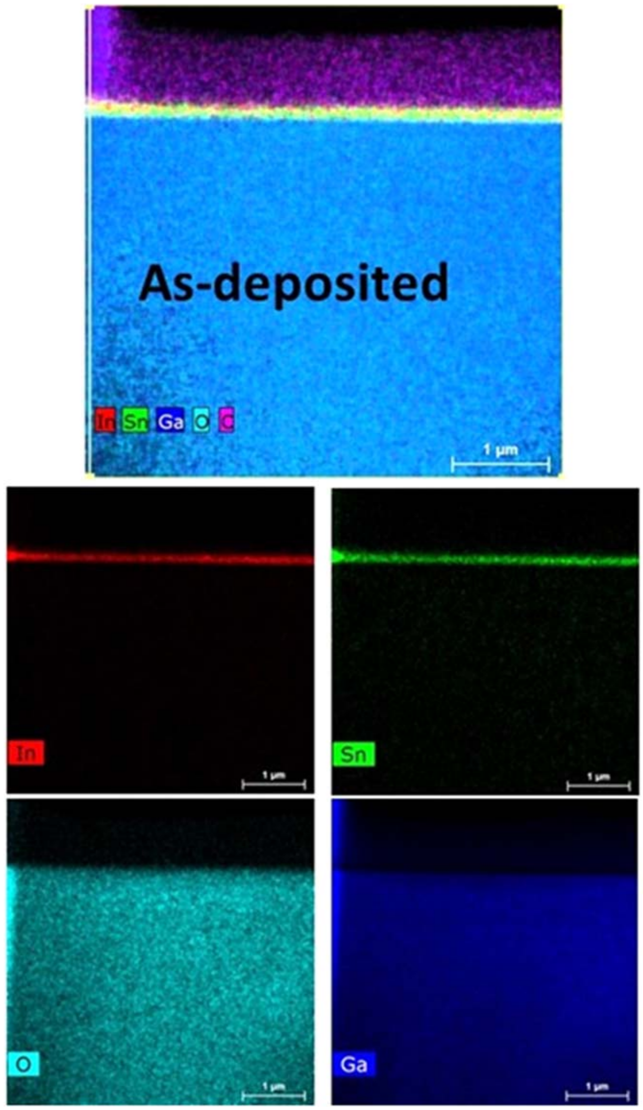

Figure 5. EDX images of the interfacial area between the ITO and Ga_2O_3 for the as-deposited samples.

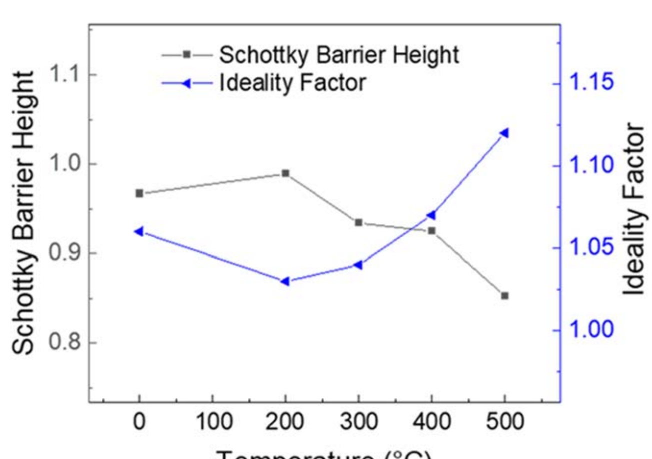

Figure 6. Schottky barrier height and diode ideality factor of ITO contacts as a function of annealing temperature in N_2 ambient.

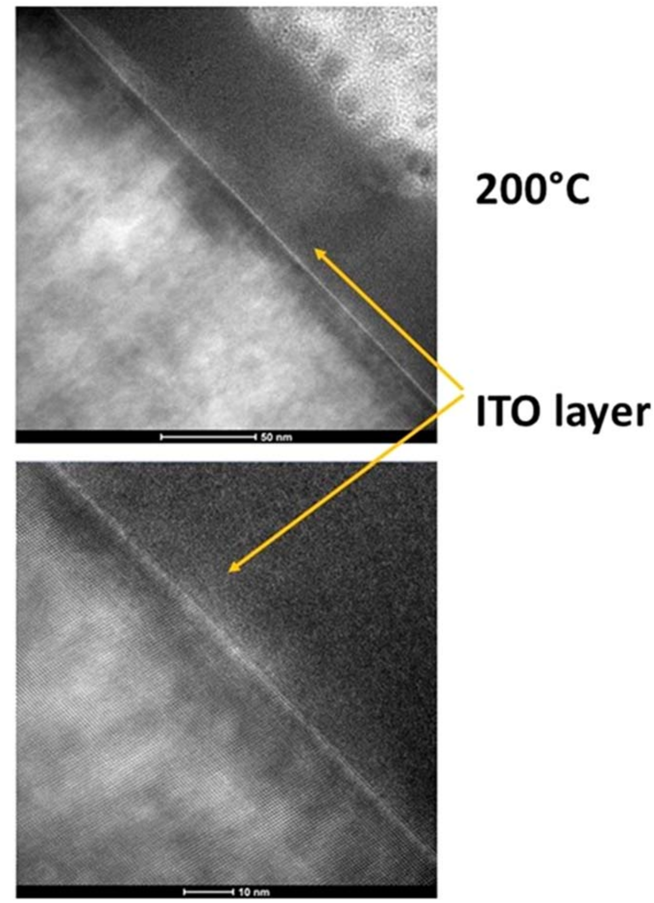

Figure 7. TEM cross-sectional images of the ITO/Ga_2O_3 interfaces after annealing at 200 °C.

ITO reacts with the Ga_2O_3 at those temperatures. Figure 4 shows cross-sectional TEM images of the as-deposited structure, with an abrupt interface between the ITO and the Ga_2O_3. This is confirmed by the EDS maps of the interfacial regions, shown in Fig. 5, where there is an abrupt transition between the Sn and In concentration profiles on either side of the interface.

Figure 6 and Table II show the Schottky barrier height and diode ideality factor of the rectifying ITO contacts as a function of annealing temperature in N_2 ambient. The ideality factor increases and the barrier height decreases with annealing temperature, consistent with the degraded interfaces seen in the TEM. As seen earlier, the ITO resistivity on Si decreases with annealing temperature, suggesting that the ITO itself is still thermally stable at these temperatures in the absence of reaction with the underlying Ga_2O_3.

TEM and EDX were again used to examine the changes in interfacial quality and composition due to the annealing. Figure 7 shows the TEM cross section after 200 °C annealing. There is no major structural changes under these conditions, consistent with the electrical measurements. After 300 °C annealing, the TEM cross section in Fig. 8 (top) shows the interface roughening, and the High Angle Annular Dark Field Imaging (HAADF), which is more sensitive to variations in the atomic number of atoms in the sample shows a reaction zone below the ITO (center). This is also clear from the EDX map (bottom), which shows reaction at the interface. This also correlates with the changes in electrical properties of both the ITO and the Schottky barrier.

The reaction is more enhanced at 400 °C, as shown in the TEM cross section of Fig. 9 and the EDX maps in Fig. 10. Under these conditions, it more difficult to delineate the ITO layer and the

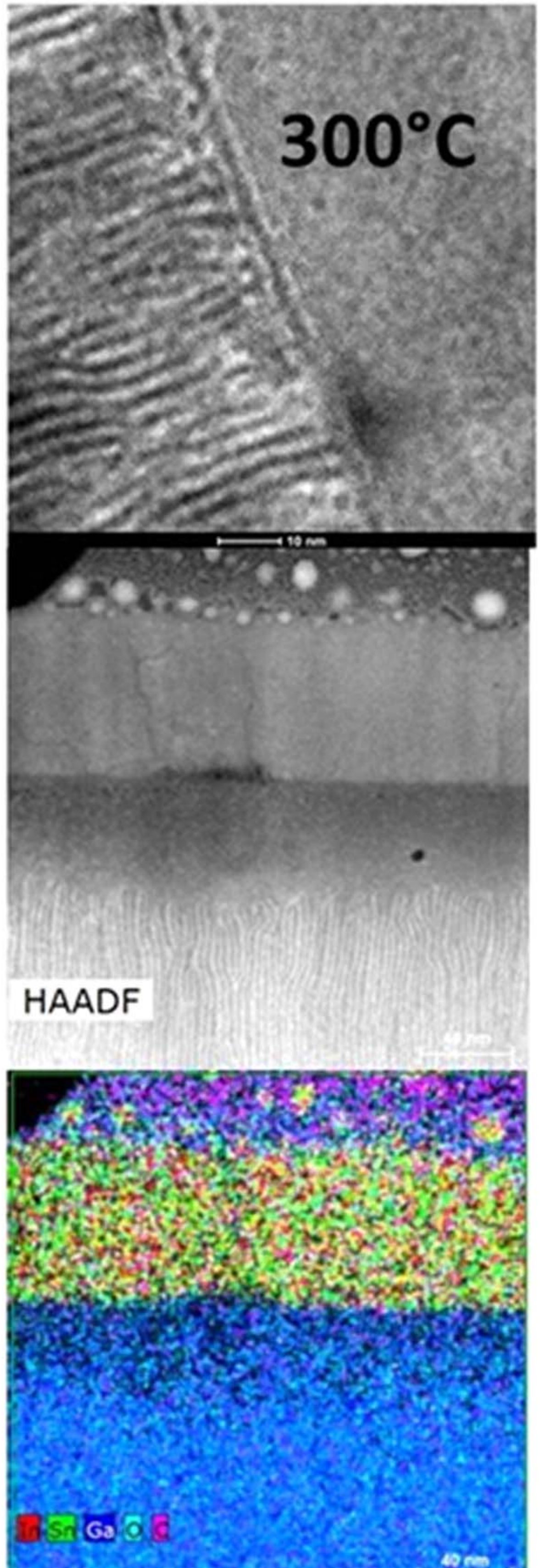

Figure 8. TEM cross-sectional image (top) HAADF image (center) and EDX map (bottom) of the ITO/Ga_2O_3 interfaces after annealing at 300 °C.

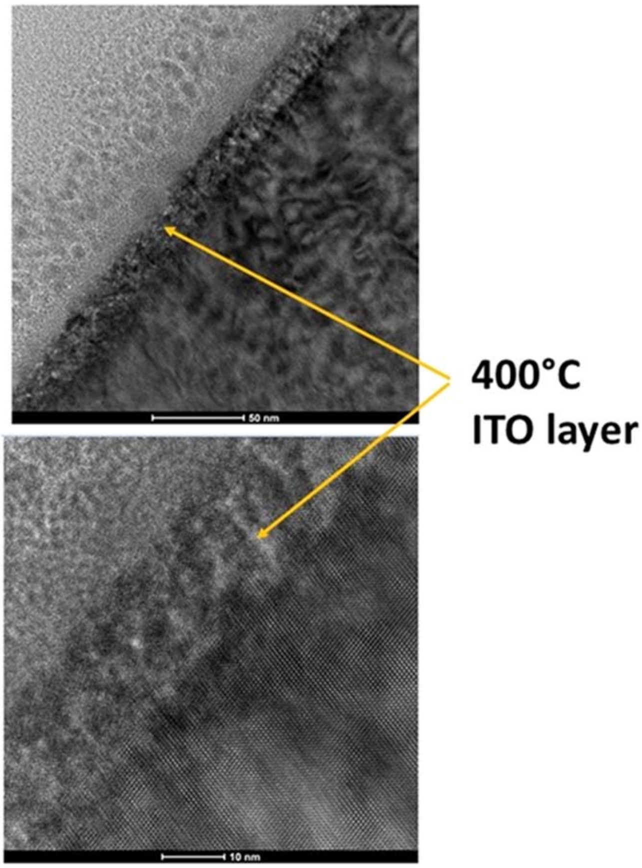

Figure 9. TEM cross-sectional images of the ITO/Ga_2O_3 interfaces after annealing at 400 °C.

compositional data shows extensive diffusion of In and Sn into the Ga_2O_3. This clearly indicates that the ITO/Ga_2O_3 interface begins to react above 300 °C and is responsible for the degradation in the I-V characteristics.

Finally, after 500 °C annealing, the TEM cross sections of Fig. 11 and the EDX images in Fig. 12 show extensive interfacial reaction and loss of integrity of the interface.

The increase in on-state resistance (Ron) with measurement temperature between 75 °C and 150 °C for Ni/Au contacts on Ga_2O_3 has been reported previously as [40,42]

$$R_{on}(T) = R_{on}(300\ K)\ (T/300)^{0.73}$$

It is also interesting to examine the annealing temperature dependence of this parameter for our ITO contacts. Figure 13 and Table III shows that R_{ON} decreases above an anneal temperature of 300 °C, which coincides with the drop in resistivity of the ITO. The specific on-state resistance of a unipolar diode is a sum of the drift region resistance, the contact resistance and the substrate resistance. Only the contact resistance will change with annealing and the reduction in ITO resistivity can account for this change. At high annealing temperatures, the reaction of the ITO with the Ga_2O_3 will lead to an increase in the on-resistance.

Figure 14 shows the reverse I-V characteristics as a function of annealing temperature, while the breakdown voltages (V_B) from these characteristics are shown in Fig. 15. The variation of V_B with annealing shows a linear dependence up to 500 °C temperature, which can be represented by a relation of the form:[28]

$$V_B = 416 + \beta(T - 25)$$

where $\beta = -0.46$ V. C^{-1}, T is the annealing temperature and 416 V is the breakdown voltage without annealing. This gives some idea of the thermal stability of the structure, in that it loses roughly 46 V in breakdown voltage for every hundred degrees increase of annealing temperature above room temperature. This indicates the breakdown voltage is one of the more sensitive indicators of contact degradation.

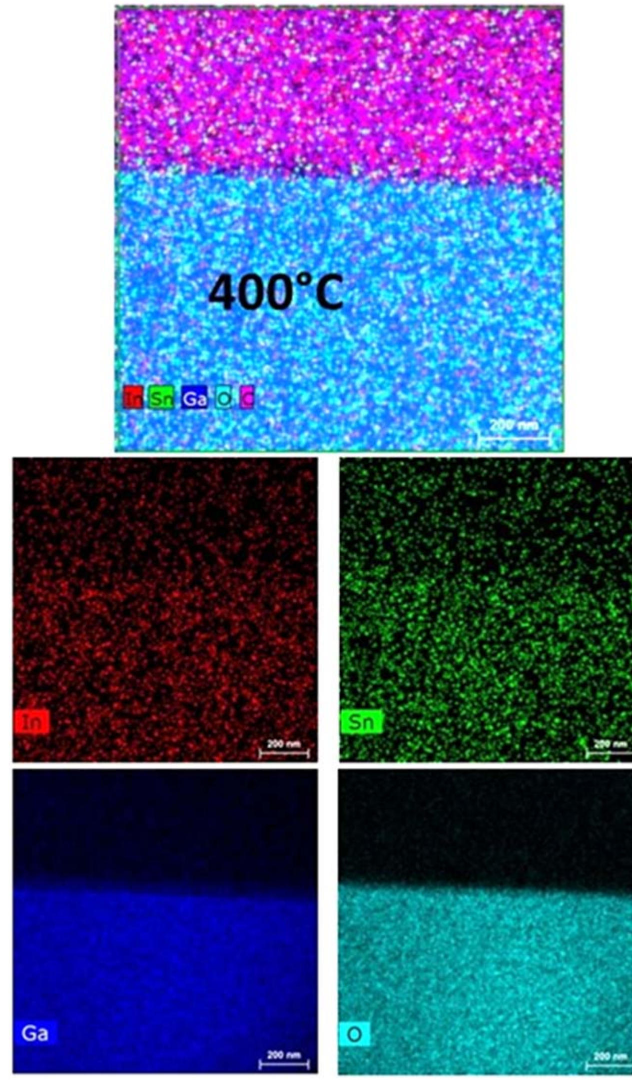

Figure 10. EDX images of the interfacial area between the ITO and Ga_2O_3 after annealing at 400 °C.

We also note that the annealing ambient did not affect the stability of the ITO/Ga_2O_3 structure over the temperature range up to 600 °C, although clearly it can affect the sheet resistance of the ITO. The reaction of the ITO with the underlying Ga_2O_3 at high temperatures proceed though interfacial reactions, although we have not yet identified the formation of any new phases in the interfacial microstructure.

Conclusions

The thermal stability of transparent, vertical Ga_2O_3 rectifiers with ITO contacts on both sides has been established. The ITO performs as a rectifying contact on lightly n-type Ga_2O_3, while it is an Ohmic contact on heavily doped n^+ Ga_2O_3. These structures are basically stable to annealing at 300 °C, beyond which the forward current density and reverse breakdown voltage suffer significant degradation. The use of ITO contacted rectifiers may have application to investigation of single event radiation upsets using laser sources to inject current and also to optically-triggered switching devices based on Ga_2O_3.

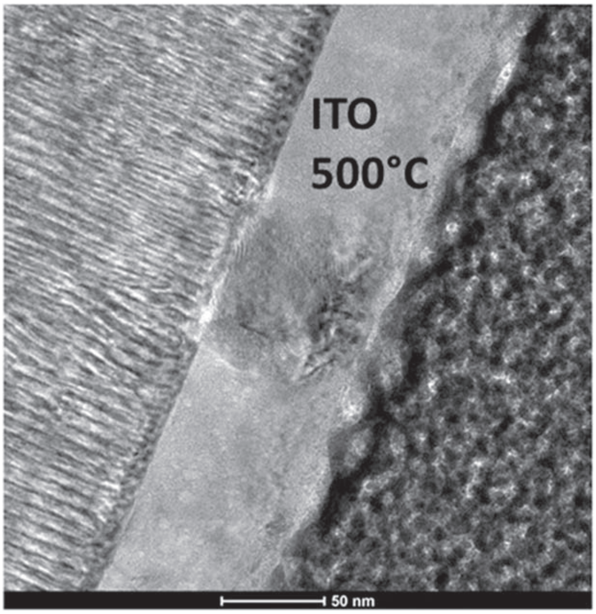

Figure 11. TEM cross-sectional images of the ITO/Ga_2O_3 interfaces after annealing at 500 °C.

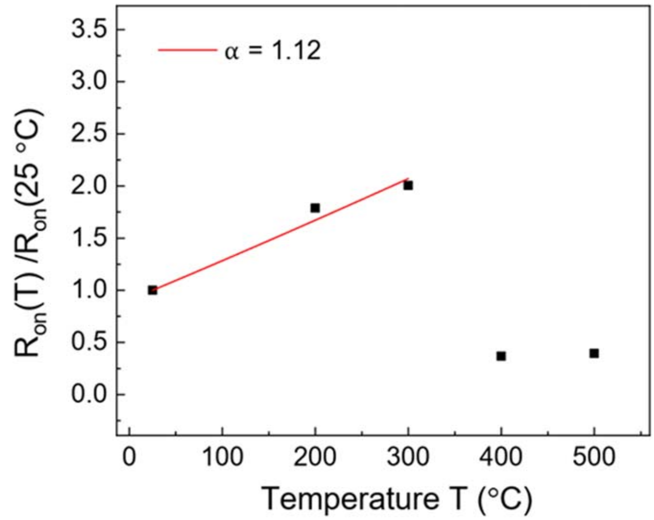

Figure 13. Plot of R_{ON} after different annealing temperatures in N_2 relative to the value at 300 K.

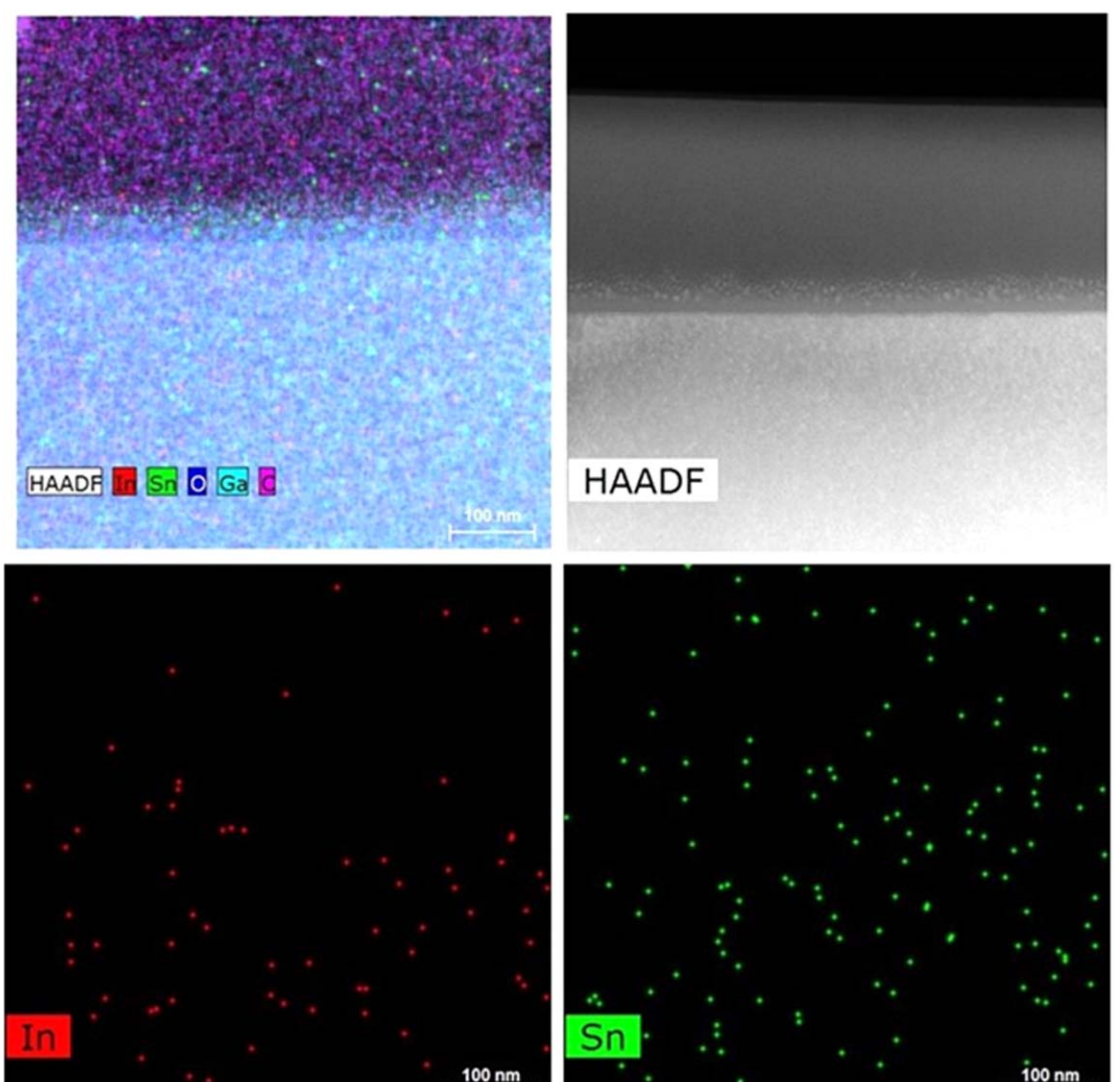

Figure 12. EDX and HAADF images of the interfacial area between the ITO and Ga_2O_3 after annealing at 500 °C.

Table III. On-resistance of ITO Schottky contacts as a function of annealing temperature.

Temperature (K)	On-resistance (mΩ·cm^2)
300	160.55
473	287.22
573	321.8
673	59.13
773	63.03

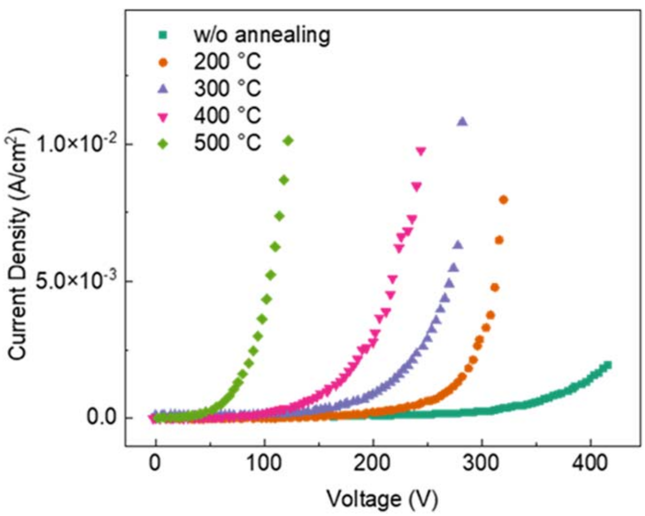

Figure 14. Reverse current density as a function of annealing temperature in N_2.

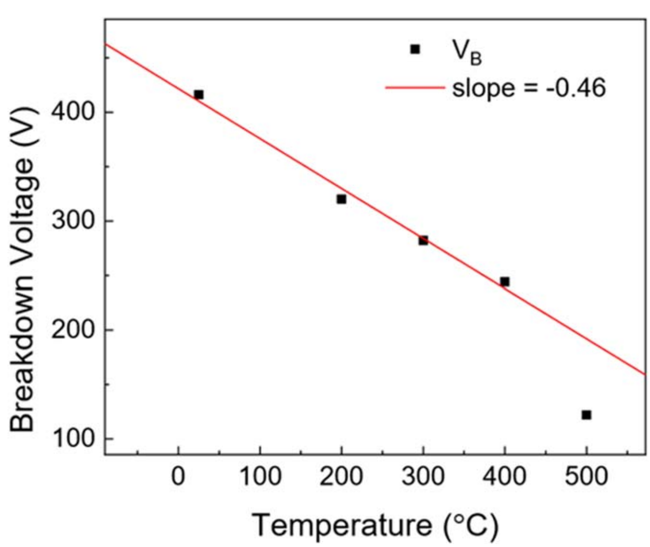

Figure 15. Reverse breakdown voltage as a function of annealing temperature in N_2.

Acknowledgments

Work performed as part of Interaction of Ionizing Radiation with Matter University Research Alliance (IIRM-URA), sponsored by the Department of the Defense, Defense Threat Reduction Agency under award HDTRA1-20-2-0002. The content of the information does not necessarily reflect the position or the policy of the federal government, and no official endorsement should be inferred. The work at UF was also supported by NSF DMR 1856662 (James Edgar). The research as PSU was partially supported by the US National Science Foundation (award # 2015795).

ORCID

S. J. Pearton https://orcid.org/0000-0001-6498-1256

References

1. S. J. Pearton, J. Yang, P. H. Cary, F. Ren, J. Kim, M. J. Tadjer, and M. A. Mastro, *Appl. Phys. Rev.*, **5**, 011301 (2018).
2. M. H. Wong and M. Higashiwaki, *IEEE Transactions on Electron Devices*, **67**, 3925 (2021).
3. X. Chen, F. Ren, S. Gu, and J. Ye, *Photonics Research*, **7**, 382 (2020).
4. E Ahmadi and Y Oshima, *J. Appl. Phys.*, **126**, 160901 (2019).
5. H. von Wenckstern, *Advanced Electronic Materials*, **3**, 1600350 (2017).
6. Z. Hu et al., *IEEE Electron Dev. Lett*, **39**, 1564 (2018).
7. J. C. Yang, F. Ren, M. J. Tadjer, S. J. Pearton, and A. Kuramata, *ECS J. Solid State Sci. Technol.*, **7**, Q92 (2018).
8. H. Zhang, L. Yuan, X. Tang, J Hu, J. Sun, Y. Zhang, Y. Zhang, and R. Jia, *IEEE Trans Power Electron*, **35**, 5157 (2020).
9. Z. Jian, S. Mohanty, and E. Ahmadi, *Appl. Phys. Lett.*., **116**, 152104 (2020).
10. M. Xiao et al., *IEEE Trans Power Electron*, **36**, 8565 (2021).
11. X. Xia, M. Xian, P. Carey1, C. Fares, F. Ren, M. Tadjer, S. J. Pearton, T. Q. Tu, K. Goto, and A. Kuramata, *J. Phys. D: Appl. Phys.*, **54**, 305103 (2021).
12. H. H. Gong, X. H. Chen, Y. Xu, F.-F. Ren, S. L. Gu, and J. D. Ye, *Appl. Phys. Lett.*, **117**, 022104 (2020).
13. W. Hao, Q. He, K. Zhou, G. Xu, W. Xiong, X. Zhou, G. Jian, C. Chen, X. Zhao, and S. Long, *Appl. Phys. Lett.*, **118**, 043501 (2021).
14. S. Bose and S. K. Mazumde, *Solid State Electron*, **62**, 5 (2011).
15. L. D. Ryder et al., *IEEE Trans Nucl. Sci*, **68**, 2496 (2021).
16. A. Khachatrian et al., *Nuclear Sci*, **62**, 2743 (2015).
17. A. Khachatrian et al., *Nuclear Sci*, **66**, 368 (2019).
18. J. M. Hales et al., *IEEE Trans Nuclear Sci*, **67**, 81 (2020).
19. A. Khachatrian et al., *Nuclear Sci*, **66**, 1682 (2019).
20. A. Khachatrian et al., *Nucl. Sci*, **65**, 269 (2018).
21. J. M. Hales et al., *IEEE Trans Nuclear Sci*, **64**, 1006 (2017).
22. L. Jianjun, Y. Jinliang, S. Liang, and L. Ting, *J. Semiconductors*, **31**, 103001 (2010).
23. S. Song et al., *Surf Sci*, **257**, 7061 (2011).
24. J. Li, L. Jiang, M. Chen, X. Li, Y. Wei, Y. Ma, Z. Fu, and Y. Yan, *Ceramics International*, **45**, 16214 (2019).
25. S. Seong, Y. C. Jung, and T. Lee, *In Sung Park, Jinho Ahn, Materials Sci. Semicond. Proc*, **79**, 14 (2018).
26. H. R. Fallah, M. Ghasemi, and H. Steki, *Mat. Res Bulletin*, **42**, 487 (2007).
27. Y. H. X. Diao, C. Wang, W. Hao, and T. Wang, *Vacuum*, **75**, 183 (2004).
28. J.-H. Park, H.-J. Seok, S. H. Jung, H. K. Cho, and H.-K. Kim, *Ceramics International*, **47**, 3149 (2021).
29. N. M. Ahmed, F. A. Sabah, H. I. Abdulgafour, A. Alsadig, A. Sulieman, and M. Alkhoaryef, *Results in Physics*, **13**, 102159 (2019).
30. X. Xia, M. Xian, P. Carey, C. Fares, F. Ren, M. Tadjer, and S. J. Pearton, *J. Vac. Sci. Technol. A*, **39**, 053405 (2021).
31. T. S. Sathiaraj, *Microelectron J*, **39**, 1444 (2008).
32. A. M. Luke et al., *J. Vac. Sci. Technol. A*, **39**, 033202 (2021).
33. L. M. Porter and J. R. Hajzu, *J. Vac. Sci. Technol. A*, **38**, 031005 (2020).
34. T. Oshima et al., *Jpn. J. Appl. Phys.*, **55**, 1202B7 (2016).
35. H. Patrick, IV. Carey, J. Yang, F. Ren, D. C. Hays, S. J. Pearton, A. Kuramata, and I. I. Kravchenko, *J. Vac. Sci. Technol. B.*, **35**, 061201 (2017).
36. R. Lingaparthi, Q. T. Thieu, K. Koshi, D. Wakimoto, K. Sasaki, and A. Kuramata, *Appl. Phys. Lett.*, **116**, 092101 (2020).
37. M. A. Mastro, C. R. Eddy Jr., M. J. Tadjer, J. K. Hite, J. Kim, and S. J. Pearton, *J. Vac. Sci. Technol A*, **39**, 013408 (2020).
38. C. Hou, K. R. York, R. A. Makin, S. M. Durbin, R. M. Gazoni, R. J. Reeves, and M. W. Allen, *Appl. Phys. Lett.*, **117**, 203502 (2020).
39. S. Ahn, F. Ren, L. Yuan, S. J. Pearton, and A. Kuramata, *ECS J. Solid State Sci. Technology*, **6**, P68 (2017).
40. M. Higashiwaki et al., *Appl. Phys. Lett.*, **108**, 133503 (2016).
41. M. Xian, C. Fares, F. Ren, B. P. Gila, Y.-T. Chen, Y.-T. Liao, M. Tadjer, and S. J. Pearton, *J. Vac. Sci. Technol. B*, **37**, 061201 (2019).
42. C. Hou, R. M. Gazoni, R. J. Reeves, and M. W. Allen, *IEEE Trans Electron Dev*, **68**, 1791 (2021).
43. P. H. Carey IV, F. Ren, D. C. Hays, B. P. Gila, S. J. Pearton, S. Jang, and A. Kuramata, *Appl. Surf. Sci.*, **422**, 179 (2017).
44. C. Buttay, C. Raynaud, H. Morel, G. Civrac, M.-L. Locatelli, and F. Morel, *IEEE Trans Electron Dev*, **59**, 761 (2012).
45. F. Wilhelmi, S. Kunori, K. Sasaki, A. Kuramata, Y. Komatsu, and A. Lindemann, *Temperature-Dependent Electrical Characteristics of a β-Ga_2O_3 Schottky Barrier Diode, PCIM Europe digital days*, **2021**, 3 (2021).
46. L. A. M. Lyle et al., *APL Mater*, **9**, 061104 (2021).
47. M.-H. Lee and R. L. Peterson, *ECS J. Solid State Sci*, **8**, Q3176 (2019).
48. M.-H. Lee and R. L. Peterson, *ACS Appl. Mater. Interfaces*, **12** 46277 (2020).
49. M.-H. Lee and R. L. Peterson, *J. Mater. Res.* (2021), (in press, 2021).
50. K. Heinselman, P. Walker, A. Norman, P. Parilla, D. Ginley, A. Zakutayev, and J. Vac, *Sci. Technol. A*, **39**, 040402 (2021).
51. M. Xian, C. Fares, F. Ren, Z. Islam, A. Haque, M. Tadjer, and S. J. Pearton, *ECS J. Solid State Sci. Technol.*, **9**, 035007 (2020).